

RESEARCH

Open Access



Modified nano magnetic Fe₂O₃-MgO as a high active multifunctional heterogeneous catalyst for environmentally beneficial carbon-carbon synthesis

Ehsan Kamali¹, Fahim Dreekvandy¹, Abolfazl Mohammadkhani¹ and Akbar Heydari^{1*}

Abstract

In this study, novel nanomagnetic catalysts, namely Fe₂O₃-MgO@choline formate (Ch. F) and Fe₂O₃-MgO@choline cyanide (Ch. CN), were synthesized through immobilizing choline-based ion liquids to magnetic support via a simple and cost-effective methodology. FT-IR, TGA, FE-SEM, VSM, EDS, BET, and XRD techniques were employed to assess and characterize these organic-inorganic compounds. Following the successful preparation of nanoparticles, the catalysts were utilized in Knoevenagel and benzoin condensations. Fe₂O₃-MgO@Ch.F. exhibited exceptional activity in Knoevenagel condensation under solvent-free conditions at room temperature, achieving high yields (91–98%) in a short timeframe. Similarly, Fe₂O₃-MgO@Ch.CN demonstrated remarkable activity in benzoin condensation under environmentally friendly solvent conditions, yielding higher isolated yields (76–88%). Furthermore, these magnetically recyclable multifunctional catalysts displayed the ability to be reused up to five times without a significant loss in efficiency. Additionally, the heterogeneity of this nanocatalyst was investigated using the hot filtration technique. The findings indicated that the reaction primarily occurs via a heterogeneous pathway.

Keywords Choline formate, Choline cyanide, Multifunctional catalysts, Nanomagnetic heterogeneous catalyst, Knoevenagel and Benzoin condensations

Introduction

In recent years, significant emphasis has been placed on developing techniques to heterogenize homogeneous catalysts while maintaining their active sites. This approach aims to amalgamate the advantages of selective, homogeneous, reactive catalysis with the recyclability and facile removal of catalysts from the reaction solution [1–9]. The coupling of homogeneous catalysts with inorganic solids is a widely utilized method for

achieving heterogeneous synthesis [1, 8, 10]. Numerous homogeneous catalysts for Knoevenagel and benzoin reactions have been explored, with these condensations being recognized for their ability to form carbon-carbon bonds [11–17]. However, homogeneous systems are associated with several drawbacks, including the high cost of catalysts, the challenge of catalyst recovery, catalyst decomposition under basic pH conditions, elevated reaction temperatures, product isolation difficulties, and the use of carcinogenic and environmentally harmful solvents, leading to substantial waste generation [18–20]. To address these challenges and preserve the catalytic active sites inherent in homogeneous counterparts, there is a growing focus on heterogenizing homogeneous catalysts [21]. This research direction has garnered significant

*Correspondence:

Akbar Heydari

Heydar_a@modares.ac.ir

¹ Chemistry Department, Tarbiat Modares University, PO Box: 14155-4838, Tehran, Iran



© The Author(s) 2024. **Open Access** This article is licensed under a Creative Commons Attribution 4.0 International License, which permits use, sharing, adaptation, distribution and reproduction in any medium or format, as long as you give appropriate credit to the original author(s) and the source, provide a link to the Creative Commons licence, and indicate if changes were made. The images or other third party material in this article are included in the article's Creative Commons licence, unless indicated otherwise in a credit line to the material. If material is not included in the article's Creative Commons licence and your intended use is not permitted by statutory regulation or exceeds the permitted use, you will need to obtain permission directly from the copyright holder. To view a copy of this licence, visit <http://creativecommons.org/licenses/by/4.0/>. The Creative Commons Public Domain Dedication waiver (<http://creativecommons.org/publicdomain/zero/1.0/>) applies to the data made available in this article, unless otherwise stated in a credit line to the data.

attention in both industrial and academic sectors. Choline chloride-based ionic liquids, such as choline azide, choline hydroxide, choline cyanide, and Choline amide serve multifaceted roles in organic processes by acting as safe, cost-effective, and efficient reactants, solvents, and homogeneous catalysts [22–28]. On the other hand, magnetic supports possess various advantageous properties, including low toxicity, cost-effectiveness, extensive surface area, Lewis acid activity, facile production, surface functionalization, rapid dispersion in processes, high conductivity, and efficient recoverability through external magnets [22, 29–36]. In the context of multifunctional catalysts for heterogeneous modification applications, it is imperative to investigate the activity of coordinated cholines on the magnetic surface. Considering the magnetic attraction and potential for agglomeration, incorporating coating stabilizers becomes necessary [37, 38]. The MgO shell acts as a shield for magnetic nanoparticles, preventing further oxidation and aggregation of the magnetic core. Notably, MgO stands out as a superior support compared to alternatives due to possessing Lewis acidic and Lewis basic sites, enabling stabilization of reaction intermediates during catalysis [39–42]. The integration of choline-based ionic liquid as a homogeneous catalyst with iron-magnesium oxide as a super-magnetic support facilitates the synthesis of highly active, multifunctional, and recyclable catalysts. These versatile catalysts are not only cost-effective and environmentally friendly but also hold significant appeal across a wide spectrum of applications. $\text{Fe}_2\text{O}_3@\text{MgO}$ effectively stabilizes choline-based ionic liquids as magnetic support in diverse applications. This study began with the novel and remarkably simple synthesis of choline formate, employing an inexpensive protocol. Subsequently, attention was directed towards investigating multifunctional heterogeneous catalysts, utilizing coordinated choline cyanides and choline formate on magnetic support. Essentially, an organo-catalyst is stabilized on the magnetic surface, exhibiting Lewis

acid and basic characteristics [43, 44]. Initial research focused on the conditions and spectra surrounding the synthesis of choline formate and choline cyanide, followed by coordinating $\text{Fe}_2\text{O}_3\text{-MgO}$ as catalysts in Knoevenagel and benzoin condensation reactions.

Results and discussion

Catalyst characterization

Figure 1 depicts the synthesis pathway of $\gamma\text{-Fe}_2\text{O}_3\text{-MgO}@$ Ch.F. and $\gamma\text{-Fe}_2\text{O}_3\text{-MgO}@$ Ch.CN. $\gamma\text{-Fe}_2\text{O}_3$ is initially produced as per the literature [41, 44–47]. To fulfill this objective, Fe_3O_4 is subjected to a reaction with ammonium hydroxide (27 wt.%) and magnesium nitrate at 70 °C for 12 h. The magnetic powder is subsequently separated and subjected to heating in a furnace for 4 h at 400 °C to yield $\gamma\text{-Fe}_2\text{O}_3\text{-MgO}$. Moreover, Ch.F. and Ch.CN are synthesized, and their magnetic surfaces are stirred at 25 °C, followed by refluxing in EtOH for 12 h at 80 °C to produce $\gamma\text{-Fe}_2\text{O}_3\text{-MgO}@$ Ch.F. and $\gamma\text{-Fe}_2\text{O}_3\text{-MgO}@$ Ch.CN, respectively. Finally, the catalysts synthesized are characterized through TGA, FTIR, FE-SEM, VSM, EDS, BET, and XRD measurements.

Figure 2 shows the FT-IR spectrum of Ch.CN, Ch.F., and $\gamma\text{-Fe}_2\text{O}_3\text{-MgO}$. In Fig. 2A, the FT-IR spectrum of Ch.CN reveals bands at 3375, 2200, 2100, 1482, 1350, and 1083, potentially attributed to OH stretching (3375 cm^{-1}), C-H bending (1482 cm^{-1}), and C–O stretching (1083 cm^{-1}). Notably, the FT-IR spectrum of Ch.CN exhibits two distinct bands, 2200 cm^{-1} (C≡N) and 2100 cm^{-1} (N–C), while the N–C peak intensities at Ch.F. are weak (Fig. 2A). Mass spectroscopy and NMR (Additional file 1: Figs. S52–S57) were employed to investigate these proposed structures, with confirmation from sedimentary tests. The FT-IR spectrum of fresh and reused catalysts reveals the Fe–O stretching vibration attributed to the iron oxide in the spinel form, observed around 569 to 584 cm^{-1} (Fig. 2A–C) [48]. In $\gamma\text{-Fe}_2\text{O}_3\text{-MgO}@$ Ch.CN, the FT-IR peak of Ch.CN (2200 and 2100 cm^{-1})

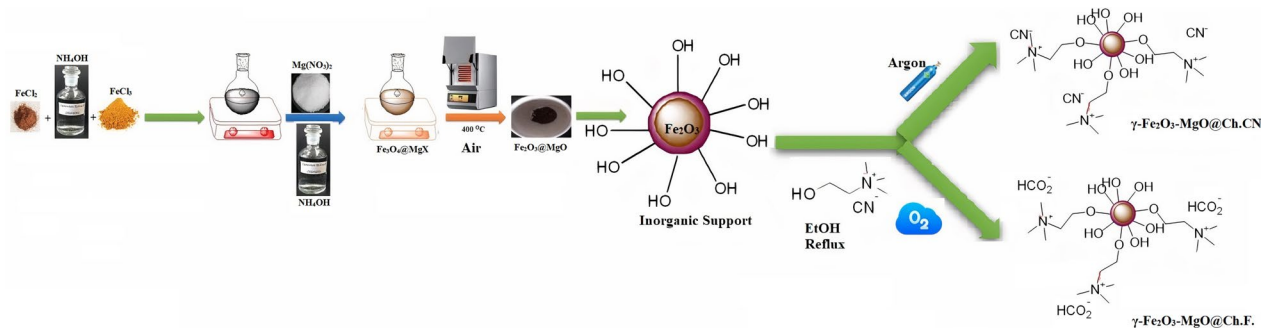


Fig. 1 Schematic diagram of catalysts preparation. The source of this diagram is taken from <https://www.nature.com/articles/s41598-023-44881-2/figures/3>. The software tools employed to create this diagram were Chemdraw and Paint. The figure was designed by authors

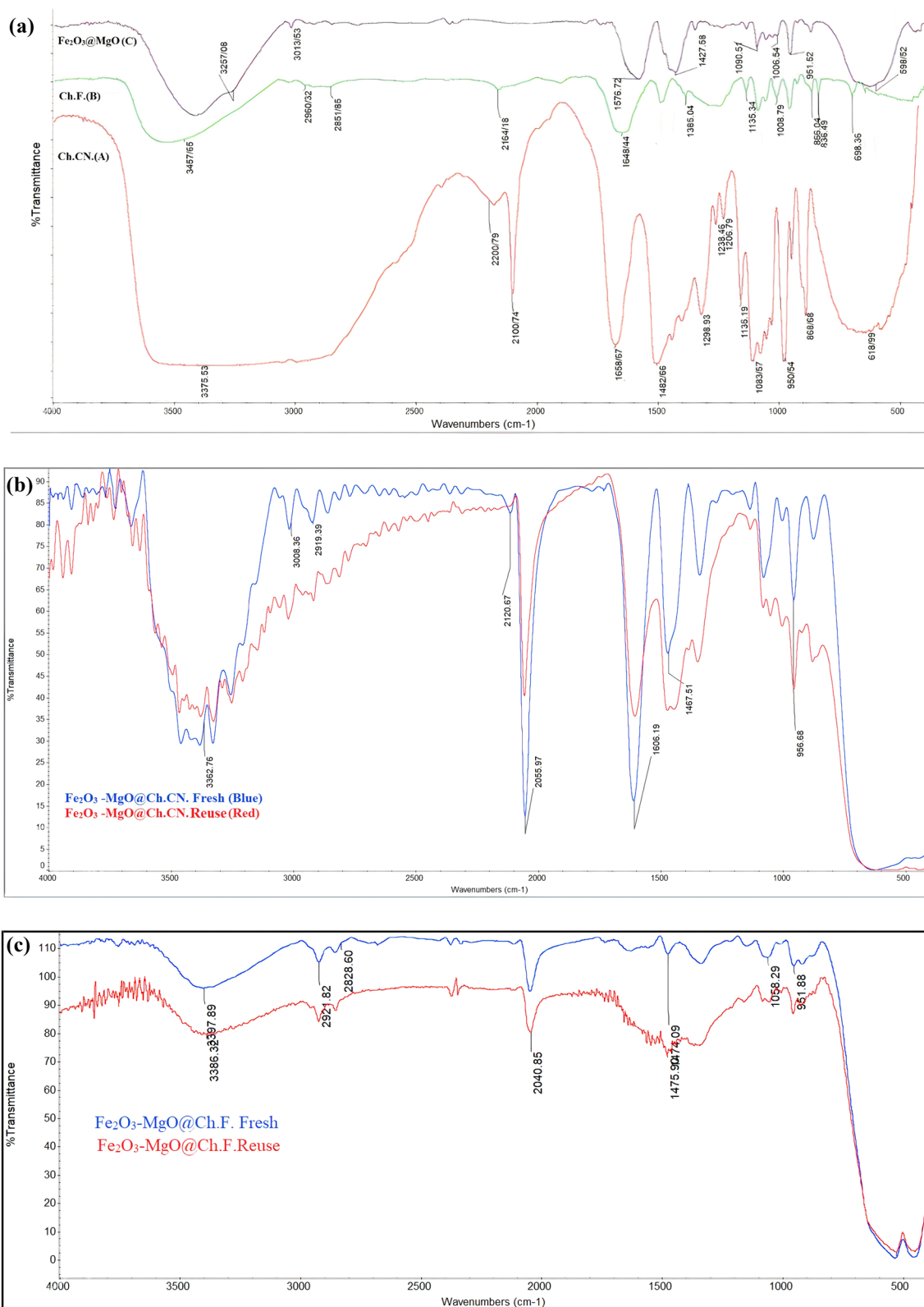


Fig. 2 A FT-IR spectrum of preparation of Ch.CN (A) Ch.F. (B) $\gamma\text{-Fe}_2\text{O}_3@MgO$ (C). B FT-IR spectrum of preparation of $\gamma\text{-Fe}_2\text{O}_3-MgO@Ch.CN$ Fresh and Reuse. C FT-IR spectrum of preparation of $\gamma\text{-Fe}_2\text{O}_3-MgO@Ch.F$. Fresh and Reuse

shifts to 2120 and 2055 cm^{-1} , respectively (Fig. 2A and B). Additionally, the FT-IR peak of Ch.F. (2164 cm^{-1}) undergoes a shift to 2040 cm^{-1} (Fig. 2A and C). This shift is attributed to the surface chelation of organic groups to $\gamma\text{-Fe}_2\text{O}_3\text{-MgO}$.

The TGA is employed for the analysis of catalyst composition and heat resistance (Fig. 3). In the cases of $\gamma\text{-Fe}_2\text{O}_3\text{-MgO@Ch.F.}$ and $\gamma\text{-Fe}_2\text{O}_3\text{-MgO@Ch.CN}$, the TGA curve indicates a minor weight loss of approximately 1–2% at 100°C , attributed to physically adsorbed water. The decomposition of organic compounds from $\gamma\text{-Fe}_2\text{O}_3\text{-MgO@Ch.F.}$ and $\gamma\text{-Fe}_2\text{O}_3\text{-MgO@Ch.CN}$ leads to a 10–12% weight loss in the temperature range of $200\text{--}400^\circ\text{C}$. Ultimately, the residual weight of 77% corresponds to $\text{Fe}_2\text{O}_3\text{@MgO}$. Thermal analysis demonstrates that the catalysts exhibit thermal stability up to 200°C (Fig. 3). Notably, the boiling points of Ch.F. and Ch.CN are 195.38°C and 190.8°C , respectively, confirming the non-sensitivity and non-energetic nature of these choline salts. DSC is employed to assess the safety of these innovative compounds in relation to chemical reactions and phase transitions as a function of temperature (Additional file 1: Figs. S1 and S2). Furthermore, no exothermic peak is observed in these experiments, with degradation occurring progressively at approximately 300°C .

FE-SEM is employed to investigate the surface morphology of fresh catalysts (Fig. 4). The images reveal the formation of spherical particles with an average size ranging from 32 to 43 nm. EDS analysis is conducted to identify the elements present in the catalysts (Fig. 5). In the case of $\text{Fe}_2\text{O}_3\text{-MgO@Ch.X}$ (X: F,CN), the EDS pattern confirms the presence of iron, magnesium, and oxygen, providing credible evidence of the modification of Fe_2O_3

by MgO. Alongside these elements, prominent peaks for carbon indicate the successful loading of choline onto $\text{Fe}_2\text{O}_3\text{@MgO}$. The Au peaks observed can be attributed to the sample holder [49].

The magnetic hysteresis loop readings for $\gamma\text{-Fe}_2\text{O}_3\text{-MgO@Ch.F.}$, $\gamma\text{-Fe}_2\text{O}_3\text{-MgO@Ch.CN}$ and $\gamma\text{-Fe}_2\text{O}_3\text{-MgO}$ are 19, 20, and 25 $\text{emu}\cdot\text{g}^{-1}$, respectively, indicating saturation magnetization. The observed decrease in saturation magnetization (MS value) may be attributed to the conversion of Fe_3O_4 into $\gamma\text{-Fe}_2\text{O}_3$ during heating and the coating of MgO on iron oxide [50]. The introduction of Ch.F. and Ch.CN onto the $\gamma\text{-Fe}_2\text{O}_3\text{-MgO}$ surface further diminishes the saturation magnetization value (Fig. 6). The effortless attraction of the nanoparticles to an external magnet further showcased their strong magnetization.

The XRD patterns of $\gamma\text{-Fe}_2\text{O}_3\text{-MgO@Ch.F.}$ and $\gamma\text{-Fe}_2\text{O}_3\text{-MgO@Ch.CN}$ are examined within the $10^\circ\text{--}80^\circ$ range to discern their crystalline structures. The XRD patterns of $\gamma\text{-Fe}_2\text{O}_3\text{-MgO@Ch.F.}$ (red line) and $\gamma\text{-Fe}_2\text{O}_3\text{-MgO@Ch.CN}$ (grey line) (Fig. 7) exhibit minimal variations. Notably, the diffraction peaks at $2\theta = 62.7, 62.2, 57.2, 53.8, 42.9, 36.8, 35.6,$ and 30 in Fig. 7, are consistent with the standard structure of $\gamma\text{-Fe}_2\text{O}_3$, as per JCPDS card No. 39-1346. Additionally, peaks at approximately $2\theta = 62.2, 50.34,$ and 18.1 are attributed to MgO (JCPDS 4-829) (Fig. 7) [46].

The specific surface area of the nanocatalysts were determined using the Brunauer–Emmett–Teller (BET) technique (Additional file 1: Fig. S6) [51]. The $\text{Fe}_2\text{O}_3\text{-MgO@Ch.CN}$ and $\text{Fe}_2\text{O}_3\text{-MgO@Ch.F.}$ have BET surface areas of 27.05 and $26.74 \text{ m}^2/\text{g}$, respectively. Incorporating Ch.F. and Ch.CN onto the $\text{Fe}_2\text{O}_3\text{-MgO}$ surface

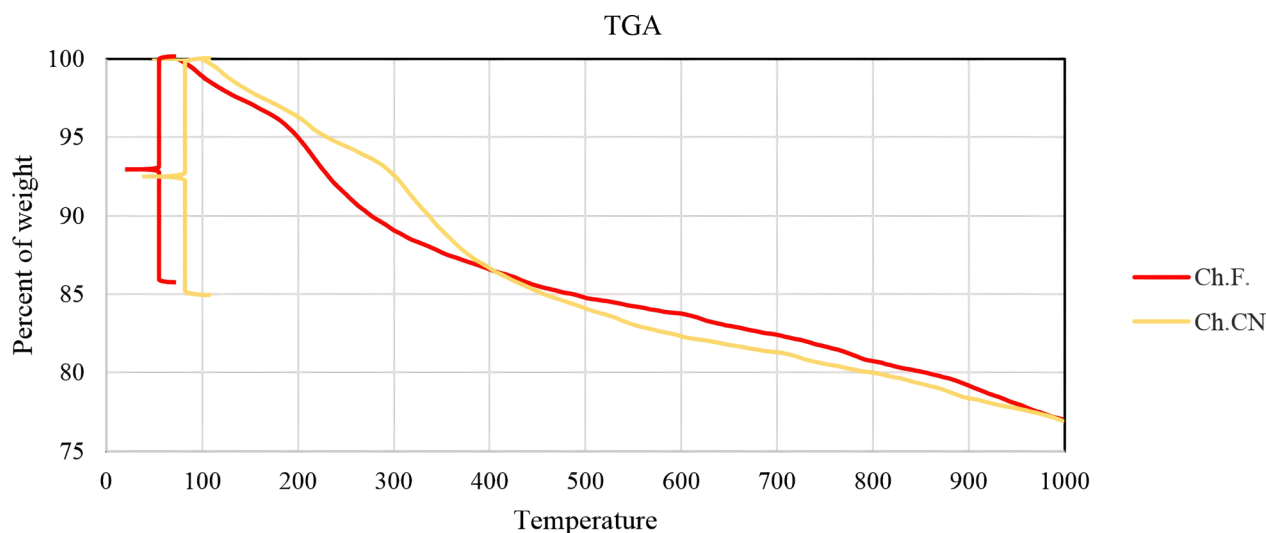


Fig. 3 TGA of $\gamma\text{-Fe}_2\text{O}_3\text{-MgO@Ch.F.}$ and $\gamma\text{-Fe}_2\text{O}_3\text{-MgO@Ch.CN}$

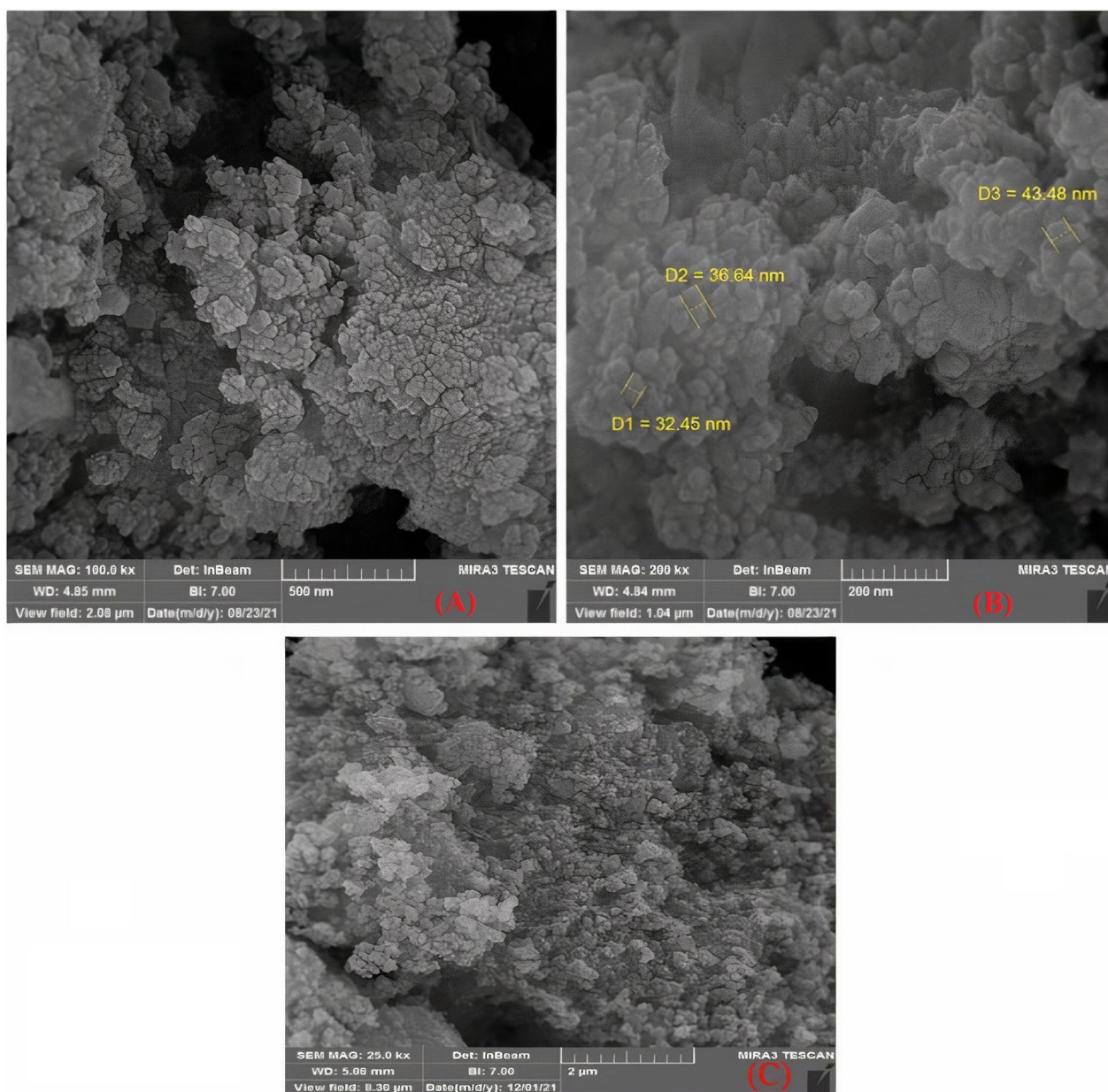


Fig. 4 SEM images of γ -Fe₂O₃-MgO (A), γ -Fe₂O₃-MgO@Ch.F. (B) γ -Fe₂O₃-MgO@Ch.CN (C)

leads to a decrease in surface area in comparison to Fe₂O₃-MgO [47].

The catalytic activity

The catalytic activity of the synthesized and characterized catalysts was evaluated in the Knoevenagel condensation using benzaldehyde 1a and malononitrile 2 as a model reaction in room temperature. Various parameters, including catalyst, solvent, catalyst loading, and reaction time, were investigated [52]. Initially, to identify the primary catalytic center of γ -Fe₂O₃-MgO@Ch.X (X:

F/CN), a model reaction was conducted in a solvent-free environment for 30 min, employing γ -Fe₂O₃-MgO, Ch.F., and Ch.CN as catalysts at room temperature. The results indicated the essential role of an organocatalyst (Ch.F. or Ch.CN) for optimal reaction efficiency. Figure 8 illustrates that the presence of γ -Fe₂O₃-MgO@Ch.F. as a heterogeneous catalyst and Ch.F. as a homogeneous catalyst resulted in higher efficiency (98%) in the model reaction. Further comparison with various Lewis acids in solvent-free and room temperature conditions revealed weak to moderate yields, with γ -Fe₂O₃-MgO@Ch.F. emerging as

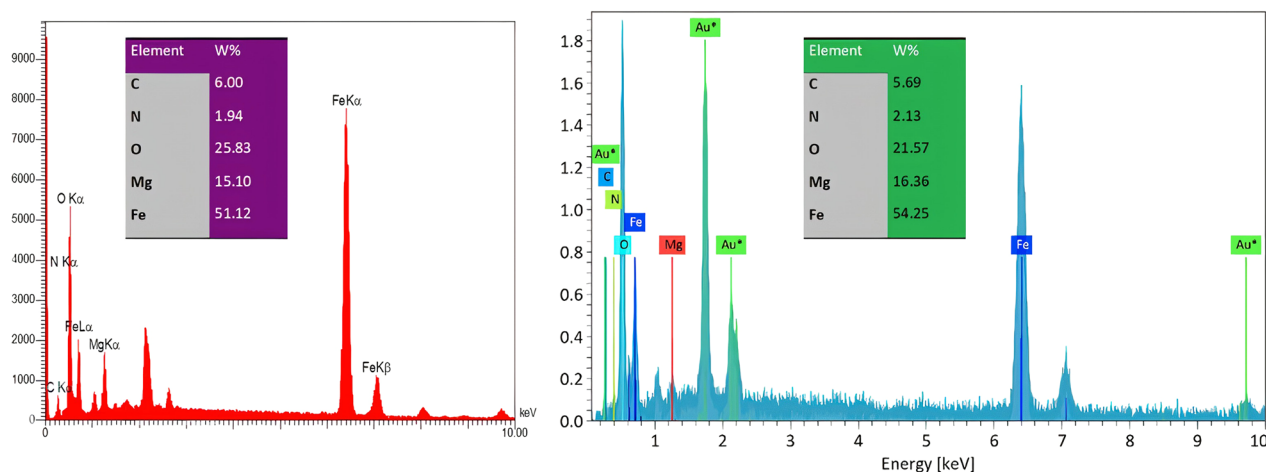


Fig. 5 EDS results of $\text{Fe}_2\text{O}_3\text{-MgO@Ch.F.}$ (Red) and $\text{Fe}_2\text{O}_3\text{-MgO@Ch.CN}$ (Blue)

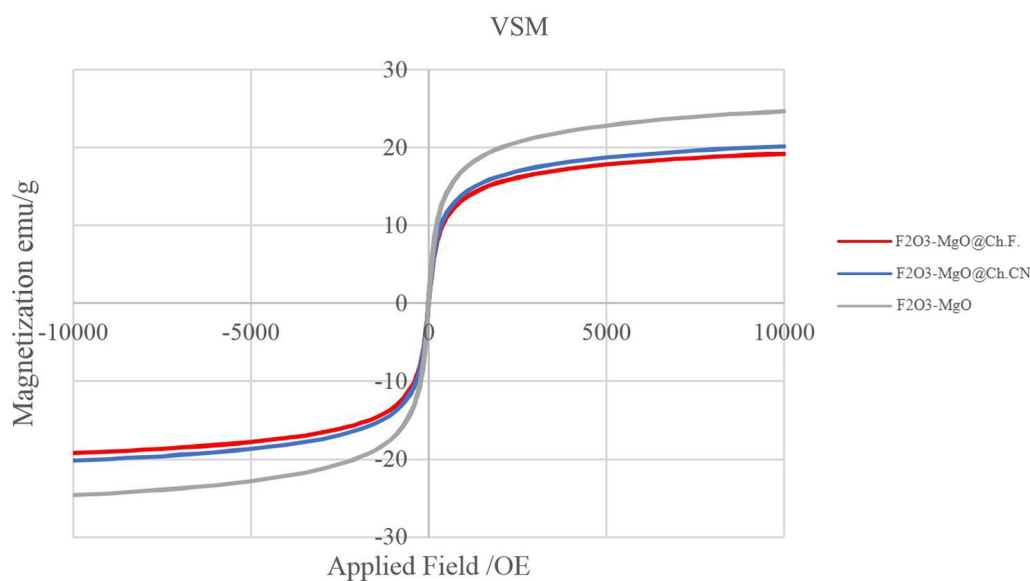


Fig. 6 VSM curve of $\gamma\text{-Fe}_2\text{O}_3\text{-MgO}$ (grey), $\gamma\text{-Fe}_2\text{O}_3\text{-MgO@Ch.F.}$ (Red) and $\gamma\text{-Fe}_2\text{O}_3\text{-MgO@Ch.CN}$ (Blue)

the preferred reusable catalyst with superior activity and the highest yield (98%) for future exploration. Exploring different solvents, such as EtOH, H_2O , MeOH, DCM, DME, THF, DCE, and toluene, with 100 mg $\gamma\text{-Fe}_2\text{O}_3\text{-MgO@Ch.F.}$ revealed yields of 62, 98, 58, 68, 23, 8, and 47%, respectively. The solvent-free condition, due to its environmental friendliness and higher efficiency (yield 98%), was determined as the optimal choice. Adjusting the catalyst mass and reaction time showed that using 100 mg of $\gamma\text{-Fe}_2\text{O}_3\text{-MgO@Ch.F.}$ and a reaction time of 30 min provided optimal conditions for higher efficiency of the target product (Fig. 8). Therefore, $\gamma\text{-Fe}_2\text{O}_3\text{-MgO@Ch.F.}$, serving as an eco-friendly, reusable, and separable

magnetic catalyst demonstrated superior efficiency under solvent-free conditions at room temperature for a short duration. Upon establishing optimal conditions, the scope of the reaction was broadened to include various aromatic and heteroaromatic aldehydes and ketones in both heterogeneous and homogeneous catalysis settings. Table 1 reveals that homogeneous systems often yield non-reusable excellent yields, while $\gamma\text{-Fe}_2\text{O}_3\text{-MgO@Ch.F.}$ consistently produces a reusable, higher output. Notably, several substituted heterocyclic ketones and aldehydes could be efficiently reacted with malononitrile to yield benzylidene malononitrile with high isolated yields (91–98%).

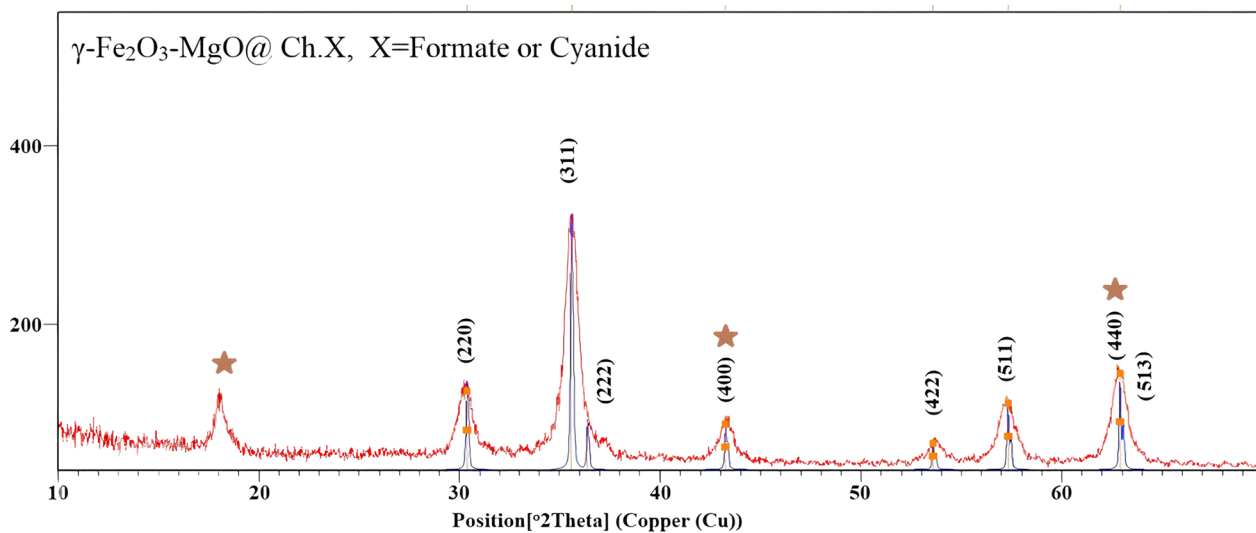


Fig. 7 XRD pattern of $\gamma\text{-Fe}_2\text{O}_3\text{-MgO@Ch.F.}$ (Red) and $\gamma\text{-Fe}_2\text{O}_3\text{-MgO@Ch.CN}$ (grey)

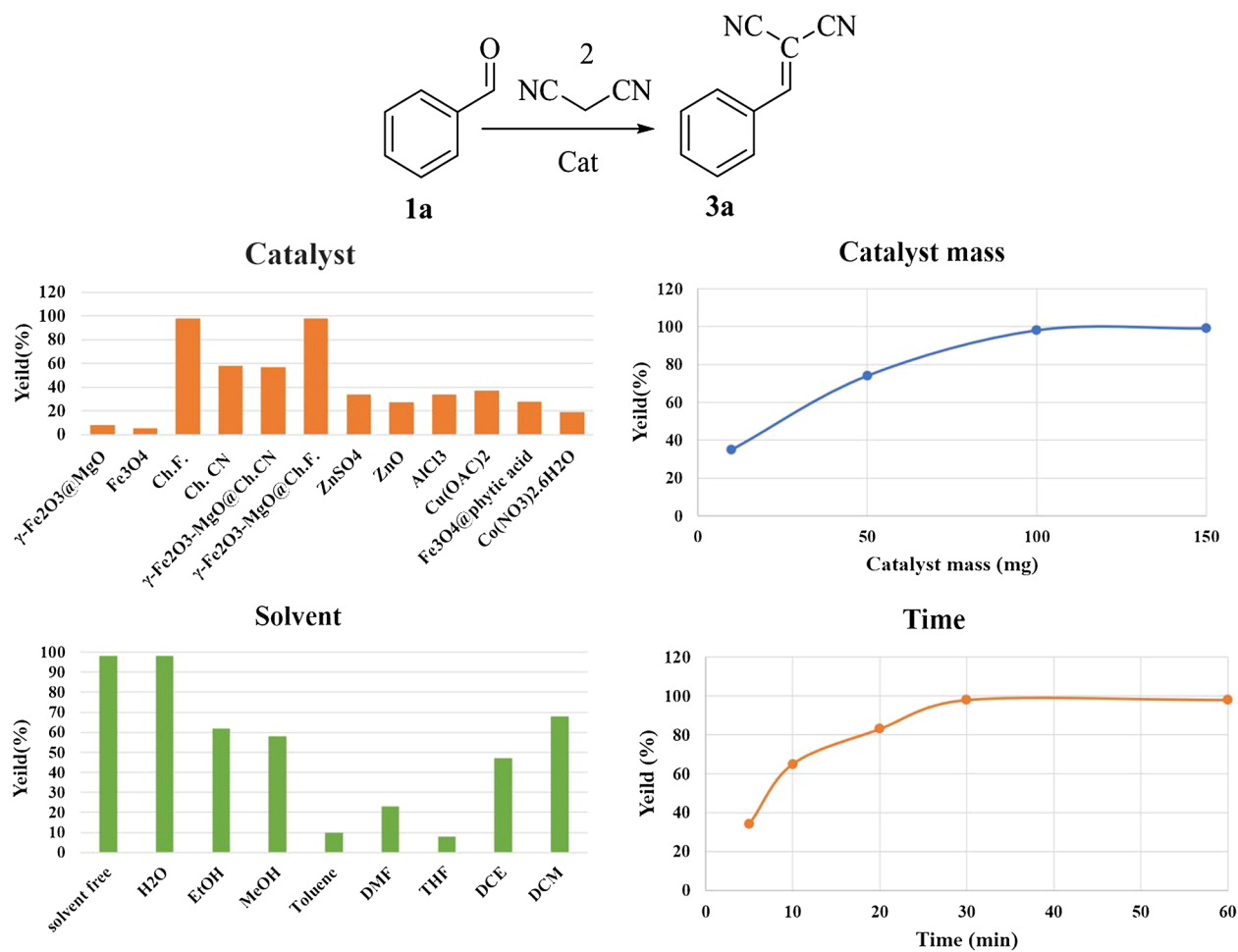


Fig. 8 Optimization of Knoevenagel condensation

Table 1 Screening of the derivatives Knoevenagel condensation

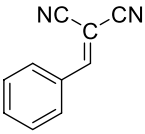
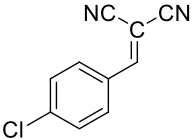
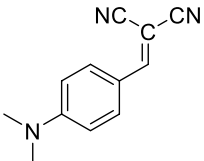
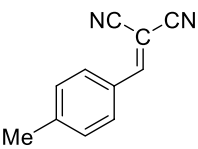
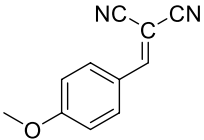
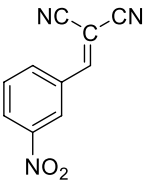
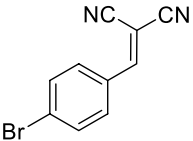
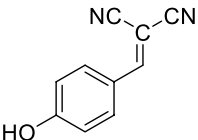
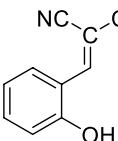
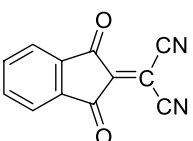
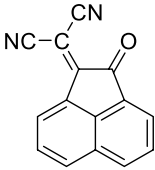
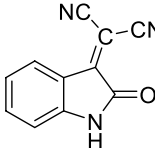
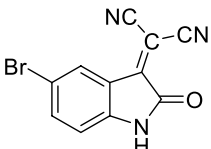
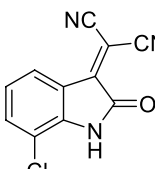
Entry	Structure	Yield(%)* γ -Fe ₂ O ₃ -MgO@ Ch.F	Yield (%)* Ch.F	M.P. (°C)	References
3a		98%	98%	82–83	[53]
3b		97%	98%	160–162	[53]
3c		97%	99%	182	[54]
3d		96%	98%	131–134	[53]
3e		97%	99%	110–112	[53]
3f		99%	99%	100–101	[55]
3g		98%	99%	165–166	[56]
3h		95%	98%	183–184	[55]
3i		95%	98%	73–74	[57]
3j		91%	93%	281	[58]

Table 1 (continued)

Entry	Structure	Yield(%)* γ -Fe ₂ O ₃ -MgO@Ch.F	Yield(%)* Ch.F	M.P. (°C)	References
3k		92%	95%	244–246	[59]
3l		94%	97%	215–217	[60]
3m		93%	95%	228–230	[60]
3n		93%	96%	245–246	[60]

*Isolated yield, Benzaldehyde (2.5 mmol), malononitrile (2.5 mmol), Cat: Ch.F.:(100 mg (0.67mmol) or γ -Fe₂O₃-MgO@Ch.F.:100mg:0.067mmol)

Encouraged by our success, we sought a new reaction to evaluate chemo-selectivity and explore choline cyanide tendencies, leading us to benzoin condensation. The model reaction involved the reaction of benzaldehyde 1a with itself under room temperature (R.T.) conditions for 1.5 h. Catalysts included Fe₃O₄, Fe₂O₃-MgO, γ -Fe₂O₃-MgO@Ch.F., Ch.F., γ -Fe₂O₃-MgO@Ch.CN, and Ch.CN and some NaCN situations were also explored. Consequently, γ -Fe₂O₃-MgO@Ch.CN emerged as the preferred reusable catalyst with superior activity (yield 88%) for further investigation (Fig. 9). Additional experiments at different temperatures revealed 25 °C as the optimal reaction temperature. Figure 9 illustrates that the rise in temperature has resulted in a decline in reaction efficiency. This decline can be attributed to the partial conversion of choline cyanide to choline formate. EtOH, H₂O, MeOH, THF, toluene, and dioxane were investigated as solvents to assess their impact on yield and reaction time. Notably, the performance of γ -Fe₂O₃-MgO@Ch.CN improved in the presence of EtOH. As depicted in Fig. 9, employing 100 mg of catalyst and a reaction time of 1.5 h proved to be optimal conditions for achieving higher isolated efficiency (88%) of the target product at room temperature. Therefore, in benzoin condensation, γ -Fe₂O₃-MgO@Ch.F. serving as an eco-friendly, reusable, and detachable

magnetic catalyst, demonstrated superior isolated efficiency under EtOH as a green solvent at room temperature for a shorter duration.

To assess the breadth of the chemo-selective reaction, various benzyl aldehydes and heteroaromatic compounds with both electron-withdrawing and electron-donating functions were screened under optimum reaction conditions, yielding high isolated efficiency (76–88%) (Table 2). Further details on the proposed methodology can be found in the accompanying material.

Recyclability γ -Fe₂O₃-MgO@Ch.F. and Fe₂O₃-MgO@Ch.CN

Hot filtration tests were conducted under optimal conditions to assess the leaching of Ch.F. from the heterogeneous catalysts during malononitrile and benzaldehyde reactions. Similarly, γ -Fe₂O₃-MgO@Ch.CN hot filtration tests were performed under ideal circumstances for benzoin condensation. In these tests, tubes were filled with EtOH after 10 and 25 min, and the catalysts were separated using an external magnet. Subsequently, the catalysts were isolated, and the reactions were terminated. No discernible improvement was observed after 45 min of stirring, as confirmed by GC analysis (Fig. 10). The results suggested that the response predominantly takes place through a heterogeneous pathway. The recyclability

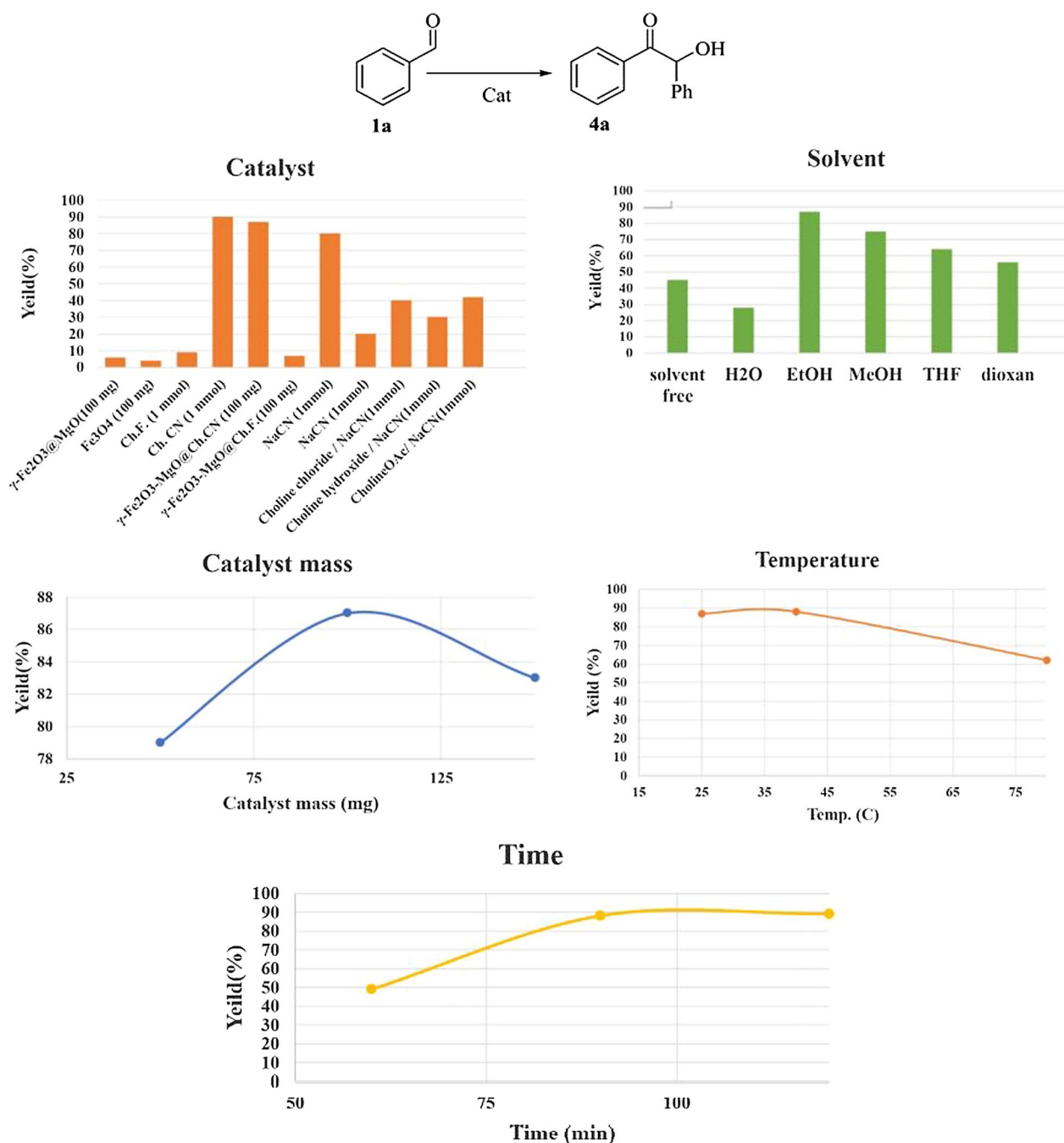


Fig. 9 Optimization of benzoin condensation

of the heterogeneous catalysts was then investigated in model reactions. Both Choline formate and cyanide heterogeneous catalysts could be regenerated for at least five cycles (Fig. 11). Following five runs, the structure of the reused catalysts was examined using FT-IR (Fig. 2B and C), XRD, FE-SEM, and VSM (Additional file 1: Figs. S3–S5). The structure of the reused $\gamma\text{-Fe}_2\text{O}_3\text{-MgO@Ch.F.}$

and $\gamma\text{-Fe}_2\text{O}_3\text{-MgO@Ch.CN}$ remained comparable to that of the fresh catalyst in all analyses.

Table 3 provides a comparative analysis of the performance of two heterogeneous catalysts employing the solvent-free condensation approach, in contrast to methodologies reported in the literature. The results highlight the remarkable efficiency of $\gamma\text{-Fe}_2\text{O}_3\text{-MgO@Ch.F.}$

Table 2 Screening of the derivatives Benzoin condensation

Label	Product	Melting point	References	Yield* Ch.CN (%)	Yield* Cat (%)
4a		132–135 °C	[61]	90%	88%
4b		65–67 °C	[61]	84%	82%
4c		94–96 °C	[61]	83%	80%
4d		76–77 °C	[62]	81%	79%
4e		109–111 °C	[61]	80%	80%
4f		134–135 °C	[63]	81%	76%
4g		107–108 °C	[64]	81%	78%
4h		239 °C	[65]	82%	77%
4i		87–89 °C	[61]	83%	79%

*Isolated yield Benzaldehyde (1 mmol), Cat:choline cyanide (1 mmol:0.13 g) or: Fe₂O₃-MgO@Ch.CN:100mg:(0.092mmol)

and γ -Fe₂O₃-MgO@Ch.CN in catalyzing condensation reactions. Notably, these catalysts address certain drawbacks associated with previously reported methods. In comparison to many earlier catalysts, the presented catalysts offer distinct advantages. They prevent the need for homogeneous catalysts, which are challenging to separate from the reaction mixture, more costly, involve hazardous organic solvents, and necessitate extended reaction times. In contrast, the protocol outlined in this study offers several benefits, including reusability, cost-effectiveness, simple preparation using readily available materials, easy separation through an external magnetic field, and the ability to achieve good to high yields within

a short reaction time. Furthermore, these catalysts operate under mild and environmentally friendly conditions, establishing their superiority over previously reported counterparts. Scheme 1 illustrated a graphical depiction of the condensation reactions aided by the synthesized nanocatalyst.

Schemes 2 and 3 depicts the proposed mechanisms for the Knoevenagel and benzoin condensations of aromatic aldehydes catalyzed by Fe₂O₃-MgO@cholin X (X:CN, F.) nanoparticles, respectively. In the Knoevenagel reaction, the nanocatalyst activates the aromatic aldehyde, initiating a nucleophilic attack by the methylene group of malononitrile. This sequence leads to the formation of

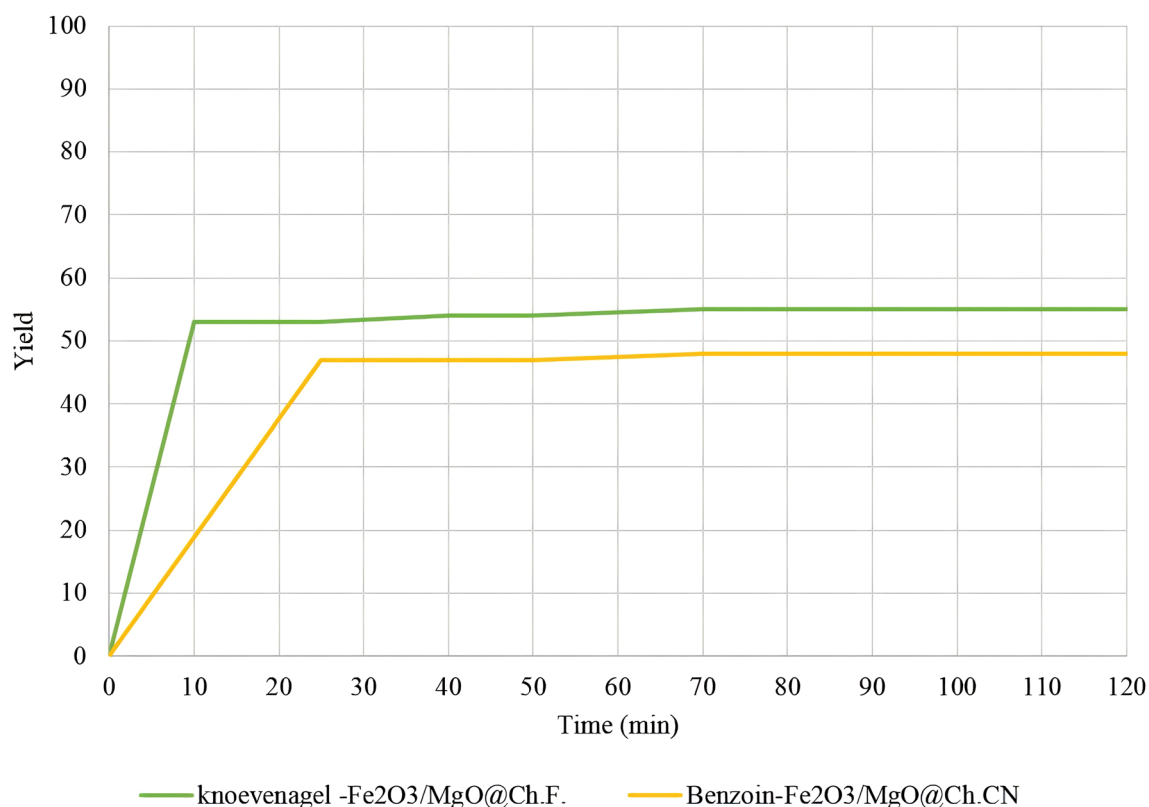


Fig. 10 Hot filtration Test

a carbon–carbon bond, followed by the dehydration of the intermediate to yield the Knoevenagel product [72]. For the benzoin condensation, the product is synthesized through a classical mechanism [73]. The activated aromatic aldehyde undergoes nucleophilic addition with

a cyanide ion, followed by the addition of a carbanion to another molecule of aldehyde. The elimination of the cyanide ion then produces benzoin as the final product. In both reactions, the nanomagnetic support with Lewis and basic sites activates the aromatic aldehydes

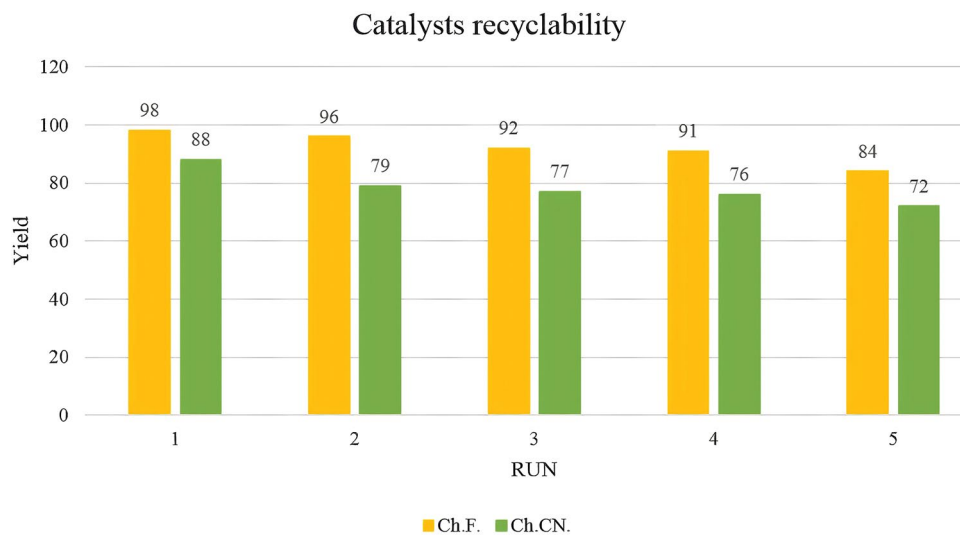
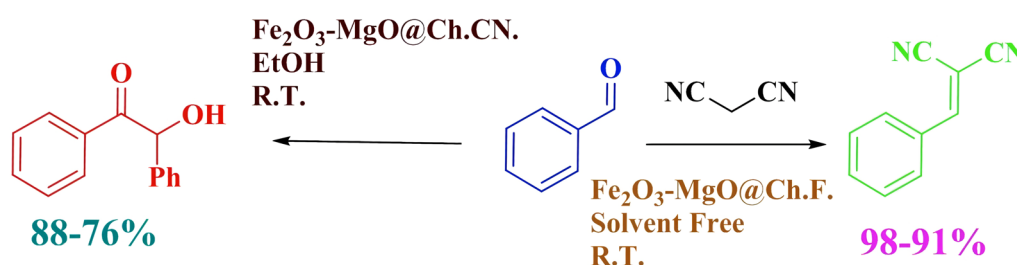


Fig. 11 Recyclability of γ -Fe₂O₃-MgO@Ch.F. and γ -Fe₂O₃-MgO@Ch.CN

Table 3 Compares the efficiency of various methods for solvent-free condensation

Entry	Time	Mol of cat	cat	Temperature	Yield	TON	TOF	Type of condensation	Reference
1	2 h	0.01 mol	Ammonium bicarbonate	90 °C	91%	1.365	0.068	K.C	[66]
2	1 h	0.005 mol	(1-((4-chlorophenyl) amino)-1-oxopropan-2-aminium perchlorate)	25 °C	97%	0.0194	0.0194	K.C	[67]
3	3 h	0.000006 mol	Zn(pcp)(aip). (H ₂ O)	25 °C	99%	32.9	10.96	K.C	[68]
4	1 h	0.2 mol	1-alkyl-2,3 dimethylimidazolium salts (NHC) and DBU(0.2)	80 °C	72%	0.0036	0.0036	B.C	[69]
5	12 h	0.5 mol	Imidazolium salts(NHC)/Cs ₂ CO ₃	30 °C	95%	0.00475	0.0004	B.C	[70]
6	5 min	0.02 mol	BMCl/NaOMe	150 °C/microwave	97%	0.53	13.2	B.C	[71]
8	30 min	0.067 mmol	γ-Fe ₂ O ₃ -MgO@Ch.F	25 °C	98%	36.56	73.13	K.C	This work
9	1.5 h	0.092 mmol	γ-Fe ₂ O ₃ -MgO@Ch.CN	25 °C	88%	4.78	3.18	B.C	This work

K.C.: Knoevenagel condensation; B.C.: Benzoin condensation



Scheme 1 Graphical abstract of condensation reactions using the synthesized nanocatalyst. The source of this diagram is taken from https://encyrted-tbn1.gstatic.com/images?q=tbn:ANd9GcT2p2AUmPXG_97tGU3HEWCr2pLuNGOZ7qSuHqu_ulo_kr632V75. The software tool employed to create this diagram was Chemdraw. The Scheme was designed by authors

and stabilizes the carbanion intermediates. The choline cation forms an ion pair with the organic moiety carrying a negative charge. The immobilization of the choline base ion liquid onto the magnetic support enhances the catalyst's reusability, making it an attractive and efficient option for these types of reactions.

Conclusions

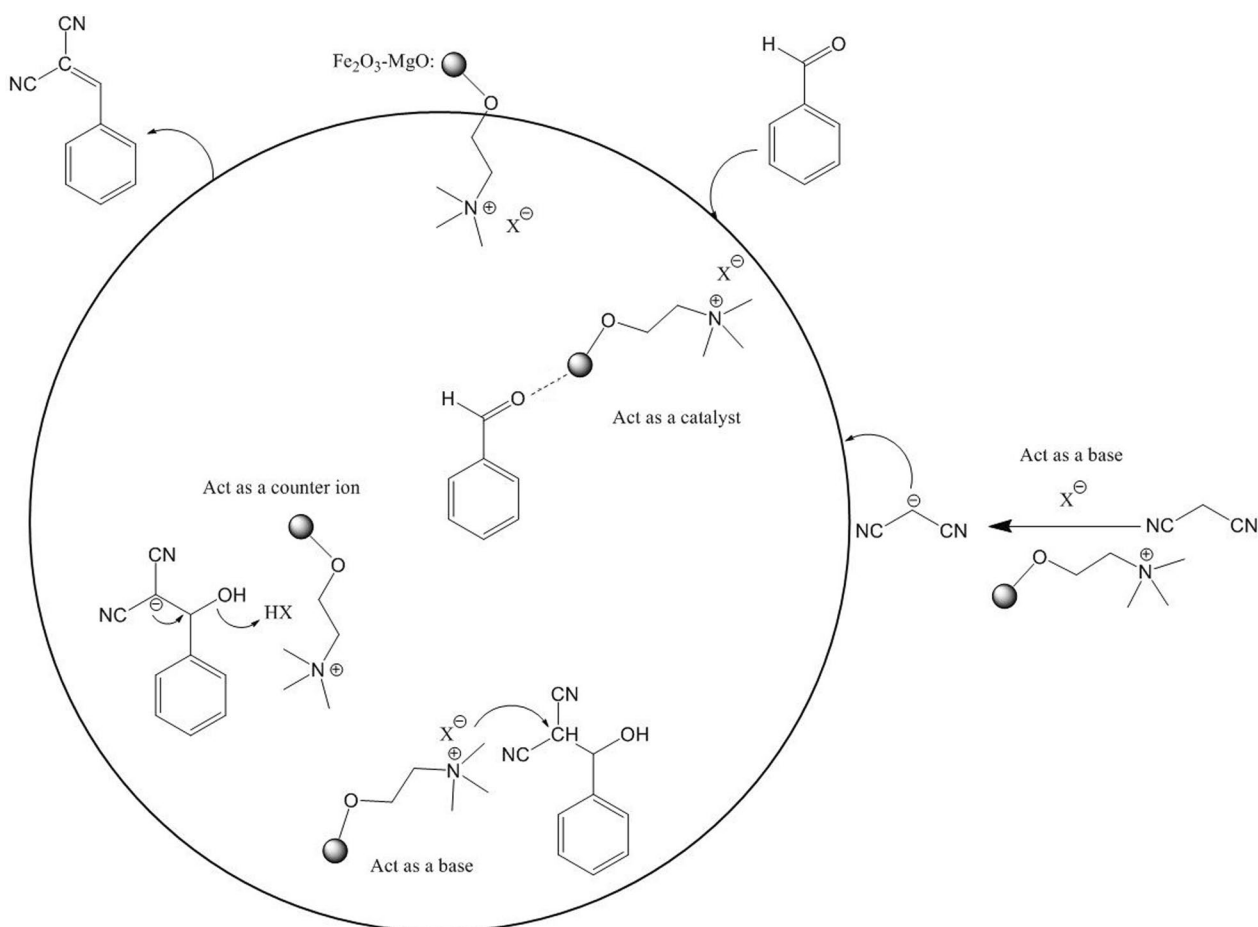
This study has successfully developed and synthesized novel super-paramagnetic multifunctional nanocatalysts. The process involved a straightforward procedure using inexpensive and readily available materials, focusing on the immobilization of homogeneous organocatalysts on magnetic support. Characterization of these nanoparticles was conducted through various techniques, including FT-IR, TGA, FE-SEM, VSM, EDS, BET, and XRD. The optimization of reaction conditions in benzoin condensations resulted in a remarkable yield of 91–98% under solvent-free and room-temperature Knoevenagel reaction conditions. Additionally, a yield of 76–88% was achieved in EtOH at 25 °C for 1.5 h in benzoin condensation, using 100 mg of the catalyst. The key advantages of this protocol encompass reusability, easy separation facilitated by

an external magnetic field, and high yield compared to similar homogeneous catalysts. Results from hot filtration tests, VSM, XRD, and SEM investigations indicate that these catalysts can be effectively reused up to five times without significant loss in efficiency. Moreover, this methodology has demonstrated effectiveness across a broad spectrum of aromatic and heteroaromatic aldehydes in both Knoevenagel and benzoin condensations.

Experimental

General

The chemicals were purchased from Merck, Aldrich, or Fluka without further purification. A BRUKERDRX-4F00AVANCE Advance spectrometer was used to record the NMR spectra. Electrothermal 9100 apparatus was used to measure melting points uncorrected. Nicolet IR100 instrument recorded IR spectra over a range of 400–4000 cm⁻¹ with spectroscopic grade KBr. Vibrating magnetometers/alternating gradient force magnetometers (MD Co., Iran, www.mdk-magnetic.com) were used for the magnetic measurement experiments. Diffraction pattern of the sample was determined using a Philips X-Pert 1710 diffraction meter.



Scheme 2 Proposed reaction mechanism for Knoevenagel condensation

A spectrum of energy-dispersive X-rays (EDX) and field emission scanning electron microscopy (FESEM). Images were recorded on Tescan MIRA3 FE-SEM. A BET analysis was conducted to ascertain the specific surface area of the composite that was prepared, utilizing the Micromeritics Instrument Corporation/TriStar II device. TGA measurements were performed on the Simultaneous Thermal Analyzer (STA 504) (www.tainstruments.com). The Mettler Toledo DSC 1 analyzer was used to carry out differential scanning calorimetry tests on choline salts.

Preparation of choline cyanide

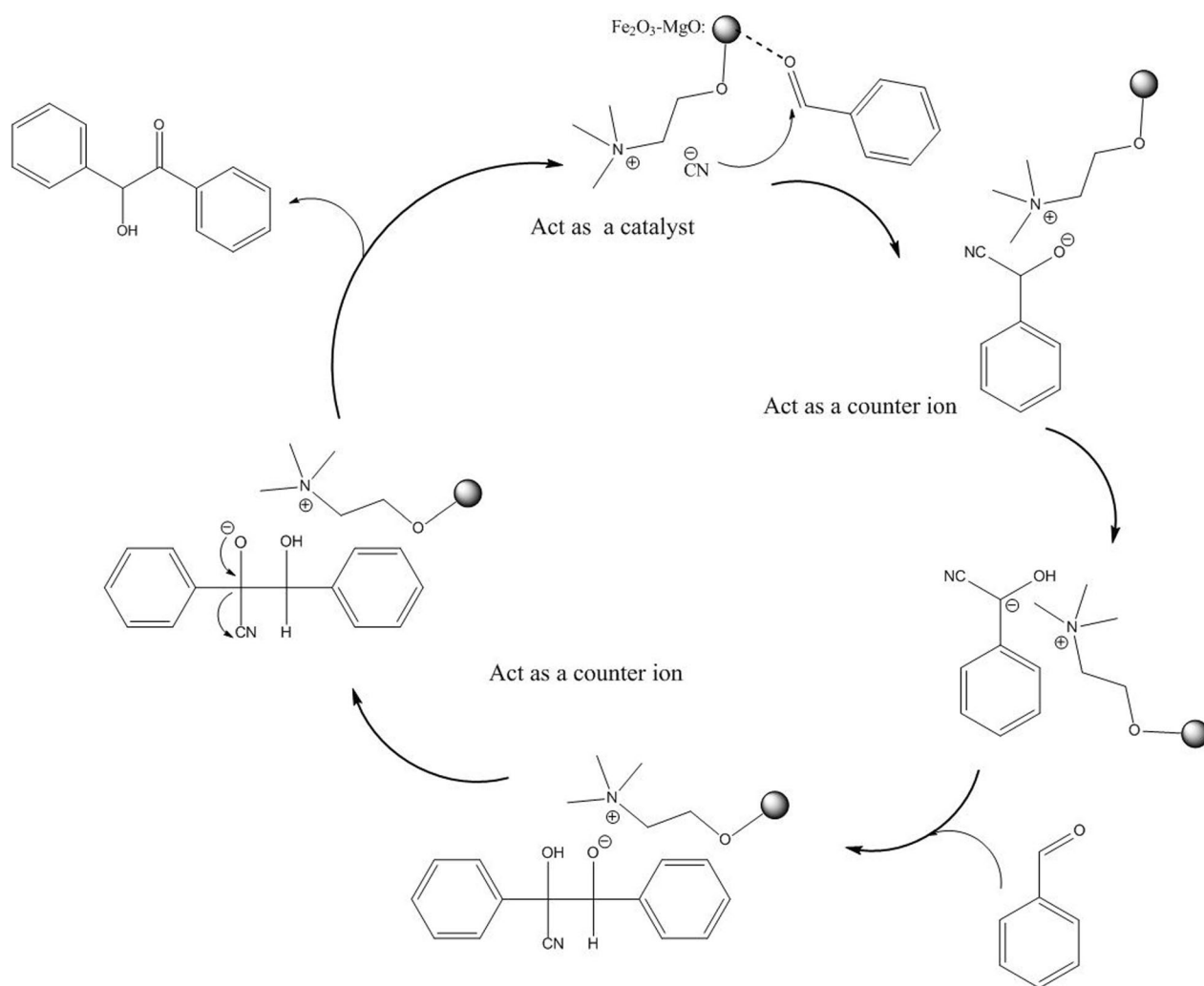
In dry-methanol (500 mL), choline chloride (1 mol) and sodium cyanide (1 mol) were refluxed for 6 h under inert condition. By ion exchange, Choline cyanide was obtained by evaporating the methanol solution under reduced pressure and filtering the sodium salts (NaCl, extra NaCN). An orange-liquid was formed.

Preparation of choline formate

In 500 mL methanol, choline chloride (1 mol) and sodium cyanide (1 mol) were refluxed for 6 h under air condition. By ion exchange, Choline formate was obtained by evaporating the methanol solution under reduced pressure and filtering the sodium salts (NaCl, extra NaCN). A red-liquid was formed.

Preparation of $\text{Fe}_2\text{O}_3\text{@MgO}$

In order to prepare Fe_3O_4 nanoparticles, 100 mL of 10 mmol $\text{FeCl}_3\cdot 6\text{H}_2\text{O}$ in 5 mmol $\text{FeCl}_2\cdot 4\text{H}_2\text{O}$ in aqueous solutions were heated to 85 °C. A drop-wise addition of ammonia (20 mL 27 weight %) was then added under stirring to reach a pH of 10–11. Following 1 h of stirring at room temperature, the black dispersion was heated to reflux for 1 h. Using an external magnet, the brown precipitate was separated. The effluent solution pH was neutralized by washing with deionized water several times. Additionally, ethanol was used to wash and suspend



Scheme 3 Proposed mechanism for benzoin condensation

the particles. Magnetite nanoparticle suspensions were sonicated with an excess of water (1:20) and magnesium nitrate or magnesium chloride (5 mmol). Under sonication for 1 h, the reaction mixture was heated, then stirred for 12 h at 70 °C under stirring. The magnet was used to separate the particles, and the ethanol was used to wash them. Afterwards, the powder was calcined at 400 °C for 4 h in air to yield γ -Fe₂O₃@MgO.

Preparation of Fe₂O₃-MgO@Ch.X

0.5 g Fe₂O₃-MgO, dry EtOH (4 mL), and choline formate (under air) or choline cyanide (under argon) (5 mmol) were stirred at 25 °C for 15 min. It was then stirred at 80 °C for 12 h. Burnt brown–red catalyst was separated by potent magnet decantation. After washing with EtOH and acetone, the catalyst was dried at 50 °C for 6 h.

Solvent-free Knoevenagel condensation procedure

A mixture of catalyst (100 mg), aldehyde (2.5 mmol), malononitrile (2.5 mmol), were stirred at 25 °C. After completion of the reaction (TLC), the magnetic catalyst was separated by an external magnet. The reaction solution was diluted with ethyl acetate (2×2 mL). The organic layer was separated and then concentrated under reduced pressure. The pure product was obtained by recrystallization with ethyl acetate: *n*-Hexane.

The general procedure for benzoin condensation

An EtOH solution was stirred with catalyst (100 mg), and aldehydes (1 mmol) at 25 °C. After the reaction (TLC), ethyl acetate was used to extract the product (2×2 mL). Separated organic layers were concentrated

under reduced pressure. A pure product was obtained by n-hexane and ethyl acetate as solvent: anti solvent.

Supplementary Information

The online version contains supplementary material available at <https://doi.org/10.1186/s13065-024-01176-5>.

Additional file 1: Supplementary Material 1.

Acknowledgements

We gratefully acknowledge the chemistry faculty at Tarbiat Modares University for supporting this work.

Author contributions

EK, FD, AM and AH designed the research project, carried out the experiments and drafted the manuscript, edited the manuscript. Additionally, EK, FD, AM and AH discussed the results and commented on the manuscript. AH led the work.

Funding

Not applicable.

Availability of data and materials

The data that supports the findings of this study are available in the supplementary material of this article. Also, All of Crude data are available at: <https://zenodo.org/record/7753834#.ZBiganZBxPY> (<https://doi.org/10.5281/zenodo.7753834>).

Declarations

Ethics approval and consent to participate

Not applicable.

Consent for publication

Not applicable.

Competing interests

The authors declare that they have no competing interests.

Received: 17 March 2023 Accepted: 28 March 2024

Published online: 20 April 2024

References

1. Abu-Reziq R, Alper H, Wang D, Post ML. Metal supported on dendronized magnetic nanoparticles: highly selective hydroformylation catalysts. *J Am Chem Soc.* 2006;128(15):5279–82.
2. Asadi B, Mohammadpoor-Baltork I, Tangestaninejad S, Moghadam M, Mirkhani V, Landarani-Isfahani A. Synthesis and characterization of Bi (III) immobilized on triazine dendrimer-stabilized magnetic nanoparticles: a reusable catalyst for the synthesis of aminonaphthoquinones and bis-aminonaphthoquinones. *New J Chem.* 2016;40(7):6171–84.
3. Biffis A, Zecca M, Basato M. Palladium metal catalysts in Heck C–C coupling reactions. *J Mol Catal A: Chem.* 2001;173(1–2):249–74.
4. Choplin A, Quignard F. From supported homogeneous catalysts to heterogeneous molecular catalysts. *Coord Chem Rev.* 1998;178:1679–702.
5. Chen J, Alper H. A novel water-soluble rhodium–poly(enolate-co-vinyl alcohol-co-vinyl acetate) catalyst for the hydroformylation of olefins. *J Am Chem Soc.* 1997;119(5):893–5.
6. Ajjou AN, Alper H. A new, efficient, and in some cases highly regioselective water-soluble polymer rhodium catalyst for olefin hydroformylation. *J Am Chem Soc.* 1998;120(7):1466–8.
7. Wang D, Wang B, Ding Y, Wu H, Wu P. A novel acid–base bifunctional catalyst (ZSM-5@Mg₃Si₄O₉(OH)₄) with core/shell hierarchical structure and superior activities in tandem reactions. *Chem Commun.* 2016;52(87):12817–20.
8. Maleki B, Taheri F, Tayebee R, Adibian F. Dendrimer-functionalized magnetic graphene oxide for Knoevenagel condensation. *Org Prep Proced Int.* 2021;53(3):284–90.
9. Saito S, Yamamoto H. Design of acid–base catalysis for the asymmetric direct aldol reaction. *Acc Chem Res.* 2004;37(8):570–9.
10. Song CE, Lee S-G. Supported chiral catalysts on inorganic materials. *Chem Rev.* 2002;102(10):3495–524.
11. Elhamifar D, Kazempoor S, Karimi B. Amine-functionalized ionic liquid-based mesoporous organosilica as a highly efficient nanocatalyst for the Knoevenagel condensation. *Catal Sci Technol.* 2016;6(12):4318–26.
12. Dumbre DK, Mozammel T, Selvakannan P, Hamid SBA, Choudhary VR, Bhargava SK. Thermally decomposed mesoporous Nickel Iron hydroxalate: An active solid-base catalyst for solvent-free Knoevenagel condensation. *J Colloid Interface Sci.* 2015;441:52–8.
13. Parida KM, Rath D. Amine functionalized MCM-41: An active and reusable catalyst for Knoevenagel condensation reaction. *J Mol Catal A: Chem.* 2009;310(1–2):93–100.
14. Varadwaj GBB, Rana S, Parida K. Amine functionalized K10 montmorillonite: a solid acid–base catalyst for the Knoevenagel condensation reaction. *Dalton Trans.* 2013;42(14):5122–9.
15. Lin Y, Lei X, Yang Q, Yuan J, Ding Q, Xu J, et al. N-Heterocyclic carbene catalyzed one-pot synthesis of 2, 3-diarylquinoxalines. *Synthesis.* 2012;44:2699–706.
16. Enders D, Balensiefer T. Nucleophilic carbenes in asymmetric organocatalysis. *Acc Chem Res.* 2004;37(8):534–41.
17. Hachisu Y, Bode JW, Suzuki K. Thiazolium Ylide-Catalyzed intramolecular aldehyde–ketone benzoin-forming reactions: substrate scope. *Adv Synth Catal.* 2004;346(9–10):1097–100.
18. Appaturi JN, Ratti R, Phoon BL, Batagarawa SM, Din IU, Selvaraj M, et al. A review of the recent progress on heterogeneous catalysts for Knoevenagel condensation. *Dalton Trans.* 2021;50(13):4445–69.
19. Kiasat AR, Badri R, Sayyahi S. Polymer supported cyanide as an efficient catalyst in benzoin condensation: an efficient route to α -hydroxy carbonyl compounds. *Bull Korean Chem Soc.* 2009;30(5):1164–6.
20. Ying A, Wang L, Qiu F, Hu H, Yang J. Magnetic nanoparticle supported amine: an efficient and environmental benign catalyst for versatile Knoevenagel condensation under ultrasound irradiation. *C R Chim.* 2015;18(2):223–32.
21. Dangolani SK, Panahi F, Nourisefat M, Khalafi-Nezhad A. 4-Dialkylaminopyridine modified magnetic nanoparticles: as an efficient nano-organocatalyst for one-pot synthesis of 2-amino-4 H-chromene-3-carbonitrile derivatives in water. *RSC Adv.* 2016;6(95):92316–24.
22. Dolatkah Z, Javanshir S, Bazgir A, Mohammadkhani A. Magnetic Isinglass a nano-bio support for copper immobilization: Cu–IG@Fe₃O₄ a heterogeneous catalyst for triazoles synthesis. *ChemistrySelect.* 2018;3(19):5486–93.
23. Lu AH, Salabas EL, Schüth F. Magnetic nanoparticles: synthesis, protection, functionalization, and application. *Angew Chem Int Ed.* 2007;46(8):1222–44.
24. Vajekar SN, Shankarling GS. Choline hydroxide promoted sustainable one-pot three-component synthesis of 1H-pyrazolo [1, 2-a] pyridazine-2-carbonitriles under solvent-free conditions. *Synth Commun.* 2020;50(8):1147–58.
25. Mehraban JA, Azizi K, Jalali MS, Heydari A. Choline azide: new reagent and ionic liquid in catalyst-free and solvent-free synthesis of 5-substituted-1H-tetrazoles: a triple function reagent. *ChemistrySelect.* 2018;3(1):116–21.
26. Shahiri-Haghayegh M, Azizi N, Heidarzadeh F. Greener and additive-free ring opening of epoxides by all-in-one choline systems. *ChemistrySelect.* 2020;5(46):14538–42.
27. Wilkes JS. A short history of ionic liquids—from molten salts to neoteric solvents. *Green Chem.* 2002;4(2):73–80.
28. Kamali E, Mohammadkhani A, Pazoki F, Heydari A. Solvent-free choline derivative synthesis as a powerful organic synthesis medium. *ChemistrySelect.* 2023;8(10): e202204642.
29. Khoshnevisan K, Vakhshiteh F, Barkhi M, Baharifar H, Poor-Akbar E, Zari N, et al. Immobilization of cellulase enzyme onto magnetic nanoparticles: applications and recent advances. *Mol Catal.* 2017;442:66–73.

30. Jia H, Zhu G, Wang P. Catalytic behaviors of enzymes attached to nanoparticles: the effect of particle mobility. *Biotechnol Bioeng.* 2003;84(4):406–14.
31. Esfandiary N, Bagheri S, Heydari A. Magnetic γ -Fe₂O₃@ Cu-LDH intercalated with palladium cysteine: an efficient dual nano catalyst in tandem CN coupling and cyclization progress of synthesis quinolines. *Appl Clay Sci.* 2020;198: 105841.
32. Ghasemzadeh MA, Abdollahi-Basir MH. Fe₃O₄@ SiO₂-NH₂ nanocomposite as a robust and effective catalyst for the one-pot synthesis of polysubstituted dihydropyridines. *Acta Chim Slov.* 2016;63(3):627–37.
33. Ghorbani-Vaghei R, Sarmast N. Green synthesis of new pyrimido [4, 5-d] pyrimidine derivatives using 7-aminonaphthalene-1, 3-disulfonic acid-functionalized magnetic Fe₃O₄@ SiO₂ nanoparticles as catalyst. *Appl Organomet Chem.* 2018;32(2): e4003.
34. Ghasemzadeh MA. Synthesis and characterization of Fe₃O₄@ SiO₂ NPs as an effective catalyst for the synthesis of tetrahydrobenzo [a] xanthen-11-ones. *Acta Chim Slov.* 2015;62(4):977–85.
35. Shylesh S, Schünemann V, Thiel WR. Magnetically separable nanocatalysts: bridges between homogeneous and heterogeneous catalysis. *Angew Chem Int Ed.* 2010;49(20):3428–59.
36. Rostamizadeh S, Tahershamsi L, Zekri N. An efficient, one-pot synthesis of pyrido [2, 3-d: 6, 5-d'] dipyrimidines using SBA-15-supported sulfonic acid nanocatalyst under solvent-free conditions. *J Iran Chem Soc.* 2015;12:1381–9.
37. Esmailipour M, Javidi J, Dodeji FN, Zahmatkesh S. Solvent-free, sonochemical, one-pot, four-component synthesis of 2 H-indazolo [2, 1-b] phthalazine-triones and 1 H-pyrazolo [1, 2-b] phthalazine-diones catalyzed by Fe₃O₄@ SiO₂-imid-PMA n magnetic nanoparticles. *Res Chem Intermed.* 2021;47:2629–52.
38. Ghasemzadeh MA, Azimi-Nasrabad M. Nano-Fe₃O₄-encapsulated silica particles bearing sulfonic acid groups as a magnetically separable catalyst for the green and efficient synthesis of 14-aryl-14H-dibenzo[a, i]xanthen-8,13-dione derivatives. *Res Chem Intermed.* 2016;42(2):1057–69.
39. Kumar JA, Amarnath DJ, Jabasingh SA, Kumar PS, Anand KV, Narendrakumar G, et al. One pot Green Synthesis of Nano magnesium oxide-carbon composite: Preparation, characterization and application towards anthracene adsorption. *J Clean Prod.* 2019;237: 117691.
40. Kaboudin B, Kazemi F, Habibi F. MgO-coated-Fe₃O₄ nanoparticles as a magnetically recoverable and reusable catalyst for the synthesis of 1-hydroxyphosphonates. *J Iran Chem Soc.* 2015;12(3):469–75.
41. De Matteis L, Custardoy L, Fernández-Pacheco R, Magén C, de la Fuente JM, Marquina C, et al. Ultrathin MgO coating of superparamagnetic magnetite nanoparticles by combined coprecipitation and sol-gel synthesis. *Chem Mater.* 2012;24(3):451–6.
42. Kaboudin B, Kazemi F, Habibi F. Fe₃O₄@ MgO nanoparticles as an efficient recyclable catalyst for the synthesis of phosphoramidates via the Atherton-Todd reaction. *Tetrahedron Lett.* 2015;56(46):6364–7.
43. Tavakol H, Keshavarzipour F. Preparation of choline chloride-urea deep eutectic solvent-modified magnetic nanoparticles for synthesis of various 2-amino-4H-pyran derivatives in water solution. *Appl Organomet Chem.* 2017;31(11): e3811.
44. Mohammadkhani A, Heydari A. Nano-magnetic-iron Oxides@ choline acetate as a heterogeneous catalyst for the synthesis of 1, 2, 3-triazoles. *Catal Lett.* 2021;152:1–14.
45. Pazoki F, Salamatmanesh A, Bagheri S, Heydari A. Synthesis and characterization of Copper (I)-cysteine complex supported on magnetic layered double hydroxide as an efficient and recyclable catalyst system for click chemistry using choline azide as reagent and reaction medium. *Catal Lett.* 2020;150:1186–95.
46. Zhang Y, Xia C. Magnetic hydroxyapatite-encapsulated γ -Fe₂O₃ nanoparticles functionalized with basic ionic liquids for aqueous Knoevenagel condensation. *Appl Catal A.* 2009;366(1):141–7.
47. Azhari A, Sh MS, Golestanifard F, Saberi A. Phase evolution in Fe₂O₃/MgO nanocomposite prepared via a simple precipitation method. *Mater Chem Phys.* 2010;124(1):658–63.
48. Arsalani N, Fattahi H, Nazarpour M. Synthesis and characterization of PVP-functionalized superparamagnetic Fe₃O₄ nanoparticles as an MRI contrast agent. *Express Polym Lett.* 2010;4(6):329–38.
49. Torres-Rivero K, Bastos-Arrieta J, Fiol N, Florido A. Metal and metal oxide nanoparticles: an integrated perspective of the green synthesis methods by natural products and waste valorization: applications and challenges. *Compr Anal Chem.* 2021;94:433–69.
50. Bhosale MA, Ummineni D, Sasaki T, Nishio-Hamane D, Bhanage BM. Magnetically separable γ -Fe₂O₃ nanoparticles: an efficient catalyst for acylation of alcohols, phenols, and amines using sonication energy under solvent free condition. *J Mol Catal A: Chem.* 2015;404:8–17.
51. Brunauer S, Emmett PH, Teller E. Adsorption of gases in multimolecular layers. *J Am Chem Soc.* 1938;60(2):309–19.
52. Kumar JA, Amarnath DJ, Kumar PS, Kaushik CS, Varghese ME, Saravanan A. Mass transfer and thermodynamic analysis on the removal of naphthalene from aqueous solution using oleic acid modified palm shell activated carbon. *Desalin Water Treat.* 2018;106:238–50.
53. Yang H, Dong H, Zhang T, Zhang Q, Zhang G, Wang P, et al. Calcined dolomite: an efficient and recyclable catalyst for synthesis of α , β -unsaturated carbonyl compounds. *Catal Lett.* 2019;149:778–87.
54. Klikar M, Kityk I, Kulwas D, Mikysek T, Pytela O, Bureš F. Multipodal arrangement of push-pull chromophores: a fundamental parameter affecting their electronic and optical properties. *New J Chem.* 2017;41(4):1459–72.
55. Zhang J, Jiang T, Han B, Zhu A, Ma X. Knoevenagel condensation catalyzed by 1, 1, 3, 3-tetramethylguanidium lactate. *Synth Commun.* 2006;36(22):3305–17.
56. Jimenez DE, Ferreira IM, Birolli WG, Fonseca LP, Porto AL. Synthesis and biocatalytic ene-reduction of Knoevenagel condensation compounds by the marine-derived fungus *Penicillium citrinum* CBMAI 1186. *Tetrahedron.* 2016;72(46):7317–22.
57. Taduri AK, Devi BR. Alum-Cs₂CO₃ as a new recyclable solid base catalyst for the efficient syntheses of arylidenemalononitriles, esters and arylcinamic acids in water. *Asian J Chem.* 2014;26(7):1938–42.
58. Junek H, Sterk H. Synthesen mit nitrilen, 19. Mitt.: die partielle retro-michael-addition von tetracyanäthylen an indandion-1, 3. *Tetrahedron Lett.* 1968;9(40):4309–10.
59. Dandia A, Jain AK, Bhati DS. Direct construction of novel dispiro heterocycles through 1, 3-dipolar cycloaddition of azomethine ylides. *Tetrahedron Lett.* 2011;52(41):5333–7.
60. Ahadi S, Yasaee Z, Bazgir A. A clean and one-pot synthesis of spiroindoline-pyranopyrazoles. *J Heterocycl Chem.* 2010;47(5):1090–4.
61. Shen G, Liu H, Chen J, He Z, Zhou Y, Wang L, et al. Zinc salt-catalyzed reduction of α -aryl imino esters, diketones and phenylacetylenes with water as hydrogen source. *Org Biomol Chem.* 2021;19(16):3601–10.
62. Demir AS, Şeşenoglu Ö, Eren E, Hosrik B, Pohl M, Janzen E, et al. Enantioselective synthesis of α -hydroxy ketones via benzaldehyde lyase-catalyzed C—C bond formation reaction. *Adv Synth Catal.* 2002;344(1):96–103.
63. Hartman W, Dickey J. The preparation of Fural. *J Am Chem Soc.* 1933;55(3):1228–9.
64. Fragnelli MC, Hoyos P, Romano D, Gandolfi R, Alcántara AR, Molinari F. Enantioselective reduction and deracemisation using the non-conventional yeast *Pichia glucozyma* in water/organic solvent biphasic systems: preparation of (S)-1, 2-diaryl-2-hydroxyethanones (benzoin). *Tetrahedron.* 2012;68(2):523–8.
65. Le ZG, Ni K, Guo LT, Xie ZB. The condensation reaction of 4-nitrobenzaldehyde and rhodanine catalyzed by papain. *Adv Mater Res.* 2014;830:111–4.
66. van Schijndel J, Molendijk D, Spakman H, Knaven E, Canalle LA, Meuldijk J. Mechanistic considerations and characterization of ammonia-based catalytic active intermediates of the green Knoevenagel reaction of various benzaldehydes. *Green Chem Lett Rev.* 2019;12(3):323–31.
67. Javle BR, Kinage AK. Chiral amino-acid-amide based ionic liquids as a stereoselective organocatalyst in asymmetric transfer hydrogenation of acetophenone at room-temperature. *ChemistrySelect.* 2018;3(9):2623–5.
68. Ma L, Wang X, Deng D, Luo F, Ji B, Zhang J. Five porous zinc (II) coordination polymers functionalized with amide groups: cooperative and size-selective catalysis. *J Mater Chem A.* 2015;3(40):20210–7.
69. Aupoix A, Pégot B, Vo-Thanh G. Synthesis of imidazolium and pyridinium-based ionic liquids and application of 1-alkyl-3-methylimidazolium salts as pre-catalysts for the benzoin condensation using solvent-free and microwave activation. *Tetrahedron.* 2010;66(6):1352–6.
70. Ema T, Nanjo Y, Shiratori S, Terao Y, Kimura R. Solvent-free benzoin and Stetter reactions with a small amount of NHC catalyst in the liquid or semisolid state. *Org Lett.* 2016;18(21):5764–7.

71. Estager J, Lévêque J-M, Turgis R, Draye M. Solventless and swift benzoin condensation catalyzed by 1-alkyl-3-methylimidazolium ionic liquids under microwave irradiation. *J Mol Catal A: Chem.* 2006;256(1–2):261–4.
72. Gilanizadeh M, Zeynizadeh B. Binary copper and iron oxides immobilized on silica-layered magnetite as a new reusable heterogeneous nano-structure catalyst for the Knoevenagel condensation in water. *Res Chem Intermed.* 2018;44:6053–70.
73. Yadav GD, Kadam AA. Atom-efficient benzoin condensation in liquid–liquid system using quaternary ammonium salts: pseudo-phase transfer catalysis. *Org Process Res Dev.* 2012;16(5):755–63.

Publisher's Note

Springer Nature remains neutral with regard to jurisdictional claims in published maps and institutional affiliations.